
Article:
Puddu, C., Rao, M. orcid.org/0000-0002-4109-4176, Xu, X. et al. (7 more authors) (2021) An asymmetrical whole-body birdcage RF coil without RF shield for hyperpolarized 129Xe lung MR imaging at 1.5 T. Magnetic Resonance in Medicine. ISSN 0740-3194

https://doi.org/10.1002/mrm.28915

Received: 23 December 2020 | Revised: 15 June 2021 | Accepted: 15 June 2021

DOI: 10.1002/mrm.28915

TECHNICAL NOTE

Magnetic Resonance in Medicine

An asymmetrical whole-body birdcage RF coil without RF shield for hyperpolarized ^{129}Xe lung MR imaging at 1.5 T

Claudio Puddu[1] | **Madhwesha Rao**[1] | **Xiaojun Xu**[1] | **Martin H. Deppe**[1] | **Guilhem Collier**[1] | **Adam Maunder**[1] | **Ho-Fung Chan**[1] | **Nicola De Zanche**[2] | **Fraser Robb**[1,3] | **Jim M. Wild**[1]

[1]POLARIS, Department of Infection, Immunity and Cardiovascular Disease, University of Sheffield, Sheffield, United Kingdom

[2]Department of Medical Physics, Cross Cancer Institute and University of Alberta, Alberta, Canada

[3]GE Healthcare, Aurora, Ohio, USA

Correspondence
Jim M. Wild, POLARIS, Department of Infection, Immunity and Cardiovascular Disease, University of Sheffield, 18 Claremont Crescent, Sheffield S10 2TA, UK.
Email: j.m.wild@sheffield.ac.uk

Funding information
Funding was provided by The Medical Research Council (MRC) grant MR/M008894/1

Purpose: This study describes the development and testing of an asymmetrical xenon-129 (^{129}Xe) birdcage radiofrequency (RF) coil for ^{129}Xe lung ventilation imaging at 1.5 Tesla, which allows proton (^{1}H) system body coil transmit–receive functionality.

Methods: The ^{129}Xe RF coil is a whole-body asymmetrical elliptical birdcage constructed without an outer RF shield to enable ^{1}H imaging. B_1^+ field homogeneity and flip angle mapping of the ^{129}Xe birdcage RF coil and ^{1}H system body RF coil with the ^{129}Xe RF coil in situ were evaluated in the MR scanner. The functionality of the ^{129}Xe birdcage RF coil was demonstrated through hyperpolarized ^{129}Xe lung ventilation imaging with the birdcage in both transceiver configuration and transmit-only configuration when combined with an 8-channel ^{129}Xe receive-only RF coil array. The functionality of ^{1}H system body coil with the ^{129}Xe RF coil in situ was demonstrated by acquiring coregistered ^{1}H lung anatomical MR images.

Results: The asymmetrical birdcage produced a homogeneous B_1^+ field (±10%) in agreement with electromagnetic simulations. Simulations indicated an optimal detuning configuration with 4 diodes. The obtained g-factor of 1.4 for acceleration factor of $R = 2$ indicates optimal array configuration. Coregistered ^{1}H anatomical images from the system body coil along with ^{129}Xe lung images demonstrated concurrent and compatible arrangement of the RF coils.

Conclusion: A large asymmetrical birdcage for homogenous B_1^+ transmission with high sensitivity reception for ^{129}Xe lung MRI at 1.5 Tesla has been demonstrated. The unshielded asymmetrical birdcage design enables ^{1}H structural lung MR imaging in the same exam.

KEYWORDS
Asymmetrical elliptical birdcage coil, hyperpolarized xenon-129, Lung RF coils

1 | INTRODUCTION

MRI of hyperpolarized gases xenon-129 (^{129}Xe) and helium-3 (^{3}He)[1,2] is established as a clinically sensitive functional imaging modality for assessment of the airways and lungs. The safety of the technique[3,4] and its inherent sensitivity to regional lung ventilation and function make it an ideal imaging tool for the assessment of lung diseases.[5,6] The method has been evaluated in clinical studies of different lung diseases and has been shown to have high sensitivity to early-stage lung diseases such as emphysema[7] and early obstruction of the airways in pediatric cystic fibrosis.[8] Due to its moderate cost and natural availability, ^{129}Xe has recently become the most employed hyperpolarized gas for MR imaging. Studies have shown that ^{129}Xe provides similar image quality and quantitative information, as can be achieved with ^{3}He MRI.[9] ^{129}Xe is also soluble in blood and tissue[10] and thus can be used to image lung ventilation–perfusion[11] and evaluate alveolar–capillary gas exchange.[12] In addition, it has been established as a useful tool for the assessment of interstitial lung disease.[13] Recently, the feasibility of ^{129}Xe-dissolved phase imaging of other perfused organs such as kidneys[14-16] and brain[17-19] has also been demonstrated. In all of these hyperpolarized ^{129}Xe applications, image quality is highly dependent on the delivered flip angle (FA); therefore, high-quality transmit RF coils capable of uniformly exciting the signal from ^{129}Xe in various organs are desirable.

In this work, we demonstrate the design and implementation of an elliptical asymmetrical thorax birdcage RF coil initially proposed for ^{3}He,[20] which has since been adopted for various applications such as sodium-23[21,22] and hyperpolarized gases.[23,24] The ^{129}Xe birdcage here was designed for the following: 1) to operate without an RF shield between the ^{129}Xe birdcage RF coil and the proton (^{1}H) system body coil to enable both ^{1}H–^{129}Xe multinuclear lung MR imaging, and 2) for use in conjunction with a dedicated receive-only RF coil array for ^{129}Xe imaging for enhanced SNR and accelerated imaging. The electromagnetic interaction of the ^{129}Xe coil with the ^{1}H body coil is an important consideration for coil performance and patient safety; thus, specific absorption rate (SAR) was evaluated with electromagnetic simulation software. In addition, transmit efficiency of the ^{1}H body coil with and without the ^{129}Xe birdcage is another necessary consideration that was optimized with electromagnetic simulation and then verified experimentally in the MR scanner. We go on to experimentally compare the ^{129}Xe birdcage RF coil when used as a transceiver and as a transmit-only RF coil in conjunction with a ^{129}Xe receive-only 8-channel RF coil array for lung ventilation MR imaging. We also demonstrate the ability to acquire coregistered ^{1}H lung images from the system body coil along with accelerated ^{129}Xe lung images.

2 | METHODS

2.1 | ^{129}Xe birdcage RF coil design and simulations

The ^{129}Xe birdcage RF coil is a 12-legged asymmetrical elliptical structure of band-pass topology, as shown in Figure 1A, similar to the topology used in an earlier ^{3}He RF coil.[25] The birdcage RF coil has length (head–feet direction) of 47 cm, common elliptical diameter (left–right direction) of 50.8 cm, asymmetrical diameter (anteroposterior direction) of 51.6 cm (top half) and 21.2 cm (bottom half), as shown in Figure 1A. The design was optimized to maximize the use of the available space within the magnet (1.5 T GE HDx scanner, GE Healthcare, Waukesha, Wisconsin), with a 60 cm inner-bore diameter used along with a custom-made patient tabletop insert. Capacitance values were calculated as described in De Zanche et al.[20] Referring to capacitors on the legs and end-rings, as shown in Figure 1A,E, the capacitor values are $C_1 = C_{12} = 450$ pF, $C_2 = C_{11} = 630$ pF, $C_3 = C_{10} = 780$ pF, $C_4 = C_9 = 680$ pF, C5 = C8 = 910 pF, $C_6 = C_7 = 580$ pF, $C_{12\text{-}1} = C_{1\text{-}2} = 1700$ pF, $C_{11\text{-}12} = C_{2\text{-}3} = 4400$ pF, $C_{10\text{-}11} = C_{3\text{-}4} = 2220$ pF, $C_{9\text{-}10} = C_{4\text{-}5} = 750$ pF, $C_{8\text{-}9} = C_{5\text{-}6} = 860$ pF and $C_{7\text{-}8} = C_{6\text{-}7} = 640$ pF.

Figure 1B illustrates the simulation environment showing the RF coils setup in the scanner. The ^{1}H system body coil has a length of 60 cm and diameter of 60.5 cm, with an outer RF shield at 63.5 cm. The proposed ^{129}Xe asymmetrical birdcage was nested inside the ^{1}H body coil. Full-wave EM simulations were performed with Ansys HFSS (Canonsburg, PA) to evaluate the following:

1. B_1^+ field homogeneity of the ^{129}Xe birdcage, for which the ^{129}Xe birdcage was loaded with human body model ($\sigma = 0.14$ S/m and $\varepsilon_r = 81$) with air spaces for lungs.
2. The ^{129}Xe birdcage RF coil was simulated for its ^{1}H RF transparency in 4 different configurations: 1 configuration without PIN diodes (tuned ^{129}Xe coil); 3 configurations with 4, 8 and 12 PIN diodes applied, respectively, to detune the ^{129}Xe coil, as shown in Figure 2. An equivalent circuit for reversed biased PIN diodes (MA4P7435NM-109IT, Macom, Lowell, Massachusetts) consisted of a 3 pF capacitance and 5 kΩ resistance in parallel. To evaluate the transparency, the RF coils were positioned in their normal operating conditions; the ^{129}Xe birdcage RF coil was set in detuned mode without excitation; and the ^{1}H body coil was tuned to the ^{1}H resonance with RF excitation to mimic the state of the RF coils during ^{1}H transmit and receive phase. The transparency of ^{129}Xe birdcage was assessed by the distortion it would cause to the ^{1}H B_1^+ magnitude and homogeneity, as shown in Figure 2.

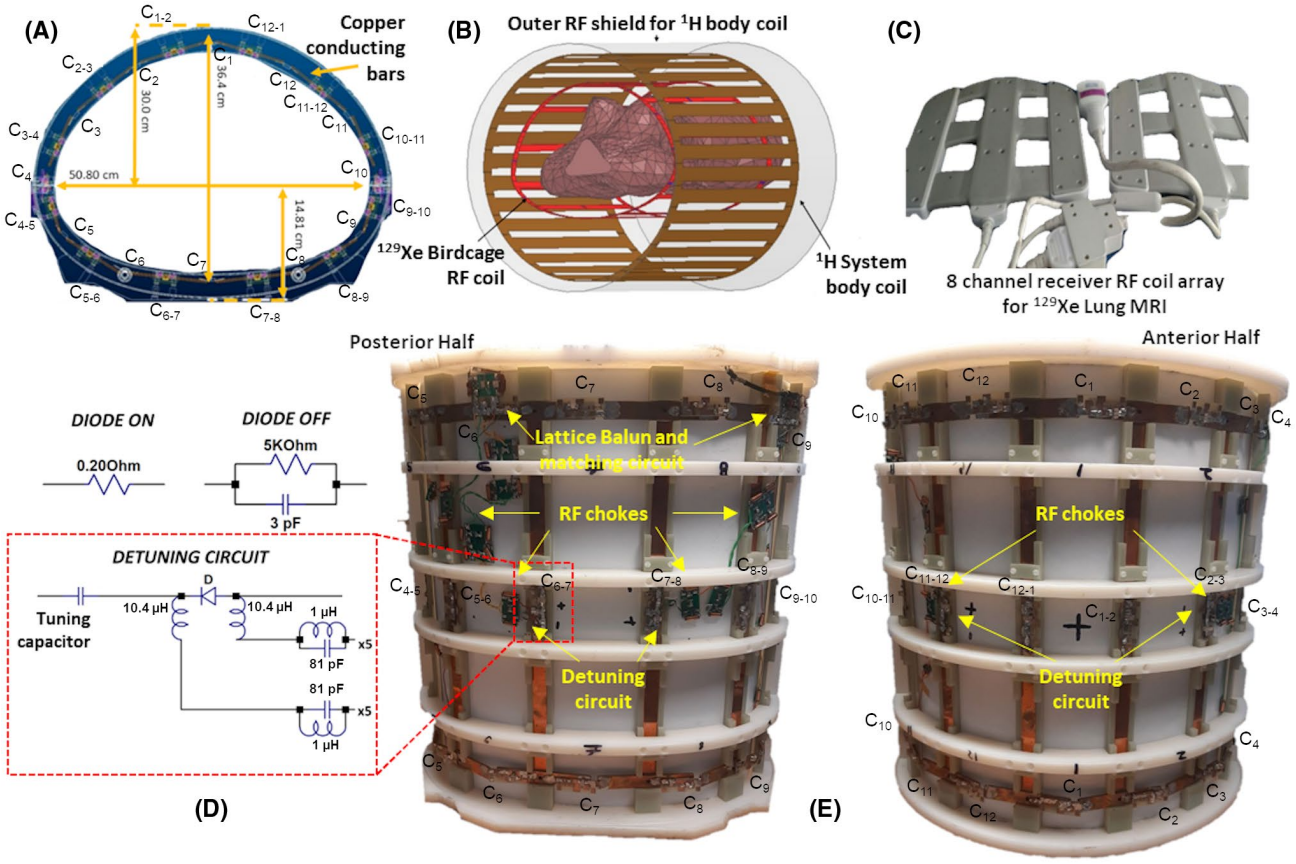

FIGURE 1 (A) Mechanical construction drawing of the ^{129}Xe birdcage RF coil, (B) simulation model of the complete RF coil arrangement that includes ^{129}Xe birdcage RF coil, system ^{1}H body coil along with its RF shield, and (C) 8-channel receiver RF coils array. (D) Detuning circuit. (E) Practically constructed ^{129}Xe birdcage RF coil, posterior/lower (left) and anterior/upper (right) half

3. The isolation s-parameters between the RF coils in all of the 4 configurations were simulated over a frequency span of 10 to 100 MHz. The ^{1}H body RF coil was tuned and the ^{129}Xe birdcage RF coil was detuned as per the diode configurations mentioned earlier. In addition, SAR was simulated in MatLab (MathWorks, Natick, MA) as described in Collins et al.[26] using the EM fields exported from Ansys HFSS 18.0 for all the 4 diode configurations mentioned.

2.2 | ^{129}Xe Birdcage coil construction

The mechanical structure of the birdcage is made from machined fiberglass composite. The conductors are solid copper bars with a length of 47 cm, width of 1.5 cm and thickness of 0.3 cm. This mechanical arrangement and its assembled geometry (shown in Figure 1A,D,E) optimally utilizes the available space and accommodates a dedicated ^{129}Xe (or ^{1}H) receiver array. The structure of the coil is split in 2 parts to allow subjects to lie down on the posterior part and the anterior part is then fixed on top. Four copper beryllium contact pins make the connection between the 2 halves. Unlike flexible coils,[27] the rigid chassis ensures a more consistent homogeneous magnetic field with loading with a range of subject sizes. Both halves of constructed RF coil are shown in Figure 1E.

The transmit RF line from the system is split into 0° and 90° channels using hybrid coupling. Each output port of the coupler was fed to the ^{129}Xe birdcage coil at quadrature using a lattice balun that also matches the RF coil to 50 Ω. The RF feeds are on the end-ring across capacitors C_6 and C_9, as shown in Figure 1E. Two cable traps tuned to ^{1}H resonance were placed on both transmit and receive cables. Active detuning was achieved by fixing 4 PIN diodes in series with capacitors $C_{2\text{-}3}$, $C_{6\text{-}7}$, $C_{7\text{-}8}$ and $C_{11\text{-}12}$ (Figure 1A,D,E), using RF chokes (10.4 µH chip inductance, parallel resonance notch circuits using 1 µH, as shown in Figure 1D).

Diode detuning was assessed by s-parameter transmission loss using magnetic flux probes with diodes turned on and off. Matching and tuning were evaluated with a human load (28-year-old male, 75 kg, 177 cm) and positioning within the scanner. Q factor was measured with the coil in the loaded and unloaded conditions.

The receiver RF coil was a repurposed ^{1}H 8-channel GE cardiac coil (GE Healthcare) retuned to resonate at the ^{129}Xe Larmor frequency of 17.66 MHz at 1.5 T (Figure 1C). The array is divided into 2 separate halves, anterior and posterior, with 4 channels each.

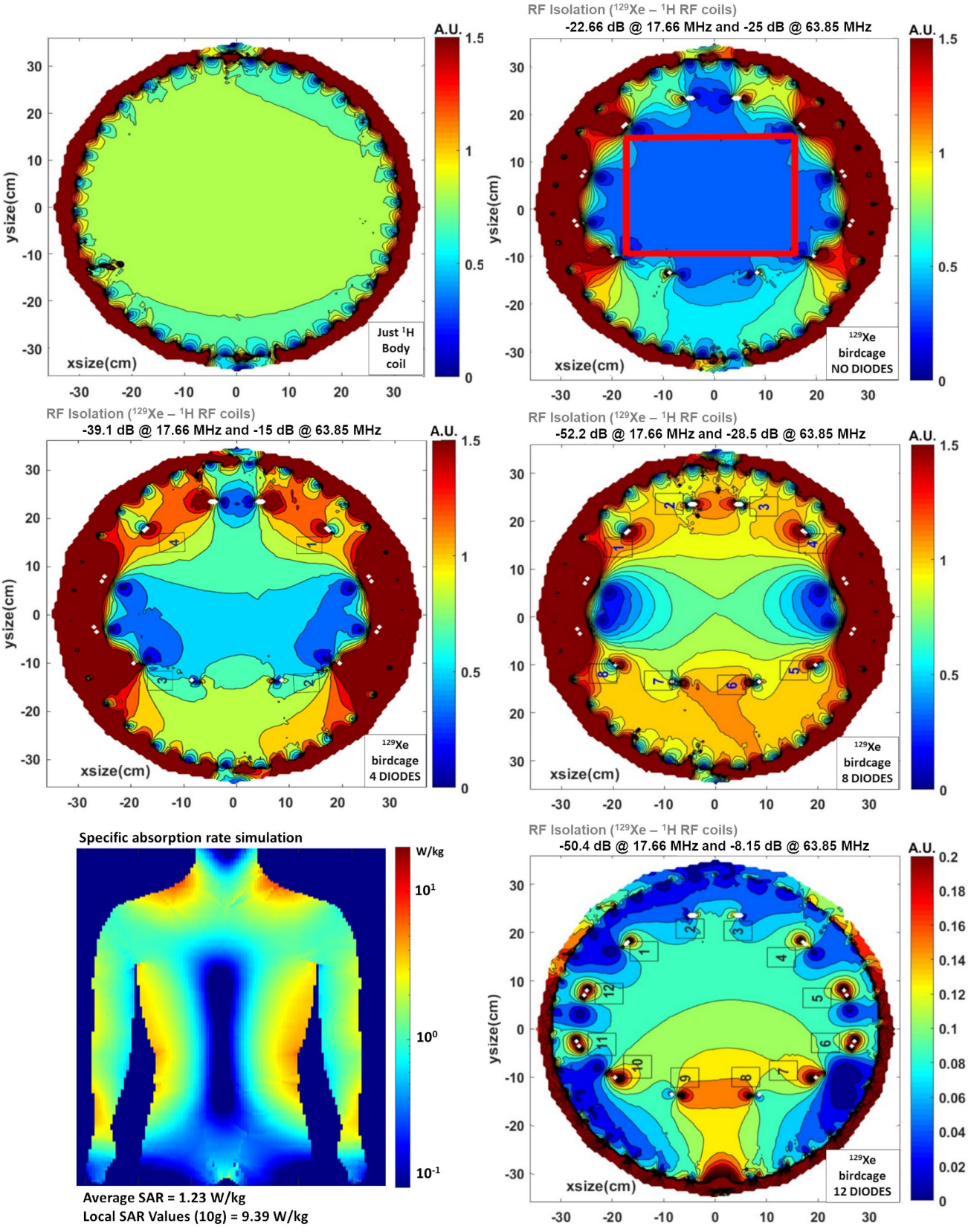
RF Isolation (^{129}Xe – ^{1}H RF coils)
-22.66 dB @ 17.66 MHz and -25 dB @ 63.85 MHz
A.U.
1.5
1
0.5
0
ysize(cm)
xsize(cm)
Just ^{1}H Body coil
^{129}Xe birdcage NO DIODES
RF Isolation (^{129}Xe – ^{1}H RF coils)
-39.1 dB @ 17.66 MHz and -15 dB @ 63.85 MHz
^{129}Xe birdcage 4 DIODES
RF Isolation (^{129}Xe – ^{1}H RF coils)
-52.2 dB @ 17.66 MHz and -28.5 dB @ 63.85 MHz
^{129}Xe birdcage 8 DIODES
Specific absorption rate simulation
W/kg
10^{1}
10^{0}
10^{-1}
Average SAR = 1.23 W/kg
Local SAR Values (10g) = 9.39 W/kg
RF Isolation (^{129}Xe – ^{1}H RF coils)
-50.4 dB @ 17.66 MHz and -8.15 dB @ 63.85 MHz
0.2
0.18
0.16
0.14
0.12
0.1
0.08
0.06
0.04
0.02
^{129}Xe birdcage 12 DIODES

FIGURE 2 Simulated B_1^+ field on the axial plane of the ^{1}H body coil at 63.8 MHz without and with ^{129}Xe birdcage RF coil nested inside for various detuning circuit configurations. The mean and SD of B_1^+ uniformity of the ^{1}H body coil within the ^{129}Xe RF coil as outlined by the red rectangle for all the configurations are 0.85% and 1.9% (without ^{129}Xe RF coil), 0.38% and 3.8% (no diodes), 0.55% and 14.3% (4 diodes), 0.85% and 20.1% (8 diodes) and 0.11% and 9.5% (12 diodes), where mean values being normalized to an obtained maximum regional value. Location of the detuning circuits on the legs in series with capacitors are marked as boxed numbers and its equivalent circuit is also shown. The RF isolation between ^{129}Xe and ^{1}H RF coils measured as transfer s-parameters (S_{21}) for all the configurations are indicated. SAR simulation for ^{1}H body coil with detuned ^{129}Xe birdcage RF coil in situ is also shown

2.3 | Hyperpolarization

Experiments were performed on a healthy male volunteer (26 years old, 70 kg) with informed written consent and approval from the UK national research ethics committee. ^{129}Xe (87% enriched ^{129}Xe) was polarized to ~ 30% by spin-exchange optical pumping[28] using a homebuilt regulatory-approved polarizer system.[29]

2.4 | FA mapping

To assess the ^{129}Xe birdcage coil homogeneity, in vivo B_1^+ maps were acquired (inhaled dose of 500 mL ^{129}Xe gas topped up with 500 mL N_2). The sequence was a 2D spoiled gradient-echo with imaging parameters: matrix resolution 32 × 32, slice thickness 200 mm, coronal/axial plane, field of view (FOV) 40 × 40 cm^2, receiver bandwidth (BW) ±4 kHz, TR = 10.2 ms and TE = 4 ms. Images from the same slice were acquired 10 times repeatedly in a short acquisition time of 4 s, thereby depolarizing the hyperpolarized ^{129}Xe gas with a known transmit RF power. The pixel-wise rate of depolarization was then used to calculate the B_1^+ maps using the relation $S_n = S_0 \sin(\alpha) \cos(\alpha)^{(n-1)}$, where S is the signal amplitude at nth RF pulse, α is the FA and S_0 is initial amplitude. To assess the RF transparency of ^{129}Xe birdcage RF coil when positioned within the ^{1}H body coil, a FA map of the ^{1}H body coil was acquired with and without the detuned ^{129}Xe birdcage RF coil in situ using a large cylindrical phantom filled with 3.6 g/L NaCl and 1.96 g/L $CuSO_4 \cdot 5H_2O$ salt solution (radius = 15.5 cm, height = 42 cm). The imaging sequence was a 2D spoiled gradient-echo, axial and coronal plane, matrix 128 × 128, TR = 300 ms, TE = 30 ms, FOV = 40 × 40 cm^2, 8 mm slice thickness and BW = 15.63 kHz. To obtain the FA map, acquisition was repeated with incremental transmit RF power and the acquired image was fitted pixelwise as described elsewhere.[30]

2.5 | ^{129}Xe ventilation imaging

The sequence used for xenon ventilation imaging was a 3D balanced steady-state free precession sequence with parameters: 100 × 82 × 24 matrix resolution, 10 mm slice thickness, BW of ±8 kHz, FOV of 40 × 40 cm^2, TR = 6.4 ms, TE = 3.1 ms, FA = 10°, and with 750 mL ^{129}Xe dose. FA was calculated with a series of pulse-acquires at a particular transmit RF power, as described earlier[28] and the average FA from all the channels were used. SNR was calculated as a ratio of average signal from the region of interest of the lungs to the square root times the SD of the background noise.[31] For the receiver array, all channels were combined with root sum of square reconstruction[32] before calculating SNR. Performance of the 2 RF coil combinations were compared using the mean SNR (Figure 4C) in a slice.

2.6 | Accelerated imaging

Array sensitivity was estimated through *autocalibration* by fully sampling the 20 lines at the center of k-space,[33] then under sampling the rest of the k-space,[34] zero-padding the unacquired k-space and reconstructing after filtering (3D low-pass Kaiser window ($\beta = 3$)[23] to prevent truncation artefacts). The optimal flip angle of the steady-state free precession varied with the number of RF encoding steps depending on the acceleration factors[35], calculated as described elsewhere,[36,37] assuming a T_1 of 20 s[38] and no off-resonance effects. The sequence used for accelerated imaging was a 3D steady-state free precession with 80 × 80 × 20 matrix, slice thickness 10 mm, BW = ±8.06 kHz, FOV = 40 × 40 cm^2, TR = 6.4 ms, TE = 3.1 ms and acceleration factor of R = 2 in the phase encode direction.

Coregistered anatomical proton MR images of the lungs were also acquired with the ^{129}Xe coils in situ; ^{1}H imaging parameters were 3D coronal spoiled gradient echo pulse sequence with matrix 80 × 80 × 20, BW = ±83 kHz; FOV = 40 × 40 cm^2, TR = 1.5 ms, TE = 0.6 ms, 5 Averages, and total scan times 12 s. Using the same parameters, a separate noise scan was performed without the inhaled gas to compute SNR. The transmit RF power for ^{1}H was limited for patient safety in accordance with the estimated SAR and RF coupling with ^{129}Xe RF coil.

3 | RESULTS

3.1 | Simulations

At 17.66 MHz B_1^+ field simulation showed a homogeneous field within the lung region with a SD of 4%. For RF

transparency of the ^{129}Xe birdcage RF coil for ^{1}H imaging, the detuning configuration with 4 diodes was optimal when compared to the other configurations despite some residual coupling that impaired the ^{1}H B_1^+ magnitude (reduction of 36%) and homogeneity (SD 14.36%), as shown in Figure 2. Simulated isolation between the ^{129}Xe birdcage coil and the ^{1}H body coil was −15 dB. Average SAR was 1.23 W/Kg and local SAR (near the shoulders) was 9.39 W/Kg simulated for ^{1}H body coil with the detuned ^{129}Xe birdcage coil in situ, as shown in Figure 2.

3.2 | ^{129}Xe Birdcage coil evaluation

Measured active detuning effectiveness (measured as difference) with diodes on and off was −23 dB at 17.66 MHz; the return loss of the ^{129}Xe transmitted birdcage was below −22 dB for both ports. The isolation between the 2 quadrature ports of the ^{129}Xe birdcage RF coil was −30.8 dB. Q factor was 197 and 100 in the unloaded and loaded conditions, respectively.

The in vivo FA delivered across the lungs with the ^{129}Xe birdcage coil had a SD of 10% and 9% for coronal and axial plane, respectively, as seen in Figure 3A,B. The FA for the ^{1}H body coil for a particular transmitted RF power with the ^{129}Xe birdcage coil in situ was 4 lower when compared without it present, as seen in Figures 3C-F.

The SNR of the birdcage when used as a transceiver versus as a transmit-only coil with 8-channel receiver RF coil array was 31, 26,18 and 46, 25, 32 in posterior, central and anterior slices, respectively (Figure 4A,B). An approximate twofold net increase of SNR was observed using the birdcage as a transmitter with receive-only RF coil array (Figure 4C). This is due to better sensitivity of the array in the anterior and posterior regions of the lungs, as seen in the SNR profile in Figure 4C.

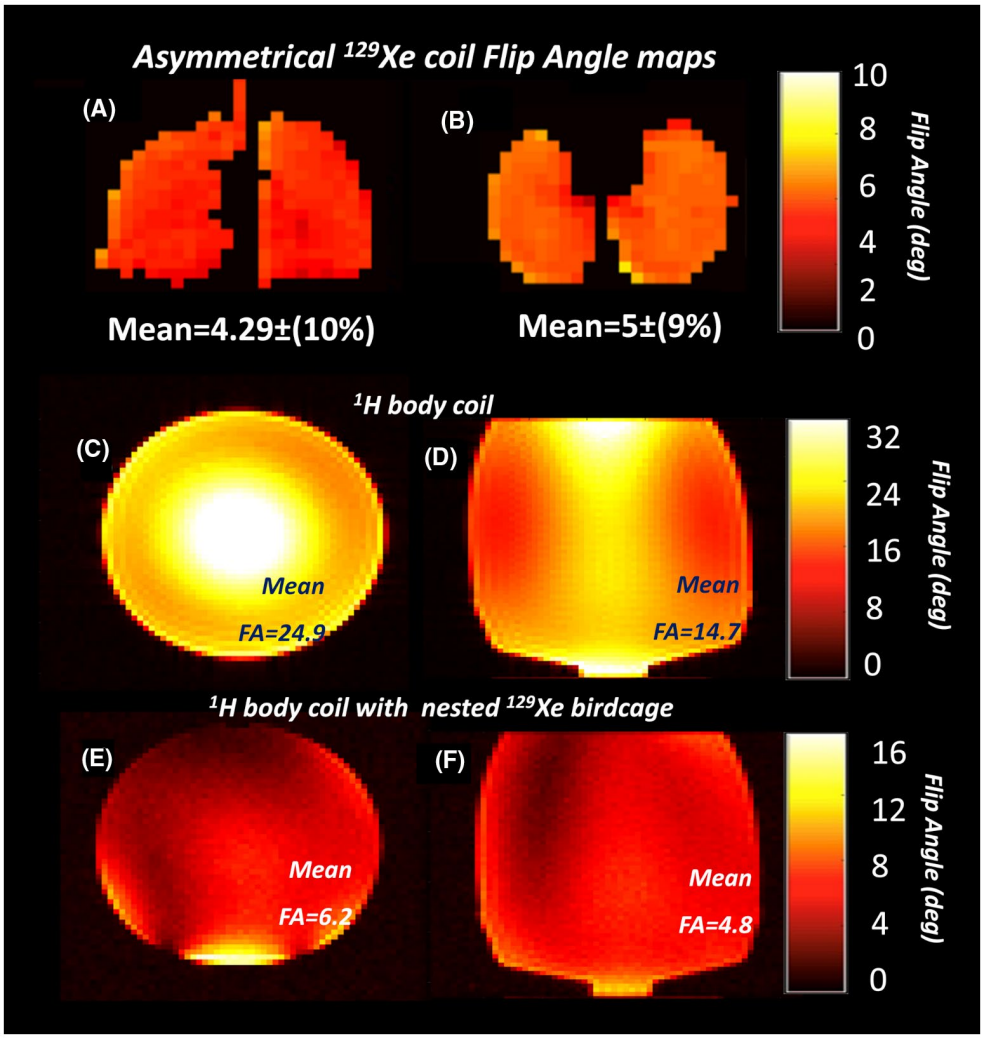

FIGURE 3 Flip angle maps of ^{129}Xe birdcage coil in vivo, (A) coronal, and (B) axial plane. Flip angle maps of ^{1}H body coil without detuned ^{129}Xe RF coil in situ, (C) axial, and (D) coronal plane. Flip angle maps of ^{1}H body coil with detuned ^{129}Xe RF coil in situ, (E) axial, and (F) coronal plane for the same transmit RF power as in (C) and (D)

^{1}H images acquired with ^{1}H system body coil with ^{129}Xe birdcage RF coil in situ enabled spatially coregistered multinuclear MR lung images (Figure 5A). HP ^{129}Xe steady-state free precession sequence signal simulations found an optimal FA of 10.3° and 14.1° for fully sampled encoded and accelerated (R = 2), respectively, as demonstrated by coronal and axial lung images reconstruction shown in Figure 5. Total scan times were 11 s and 8 s and for full sampled and R = 2 sampled, respectively. Image reconstruction for R = 2 (Figure 5B) shows no visible reconstruction artefacts with a g-factor of 1.4 (Figure 5C).

4 | DISCUSSION

In this note, we have demonstrated an asymmetrical band pass birdcage for hyperpolarized ^{129}Xe MRI that works without an RF shield enabling in situ ^{1}H imaging. In vivo FA mapping demonstrated B_1^+ similar to values reported in the literature.[24,39] Of the diode configurations evaluated for detuning, the configuration with 4 diodes showed least distortion of the ^{1}H B_1^+ field. Although the ^{129}Xe transmit birdcage coil enables proton imaging, the obtained FA with the ^{129}Xe coil in situ was lower by a factor of 4 for the same transmit power, which is likely due to residual undesired coupling between the RF coils. Increasing the transmit power of the ^{1}H RF amplifier is not an optimal solution to mitigate this because the local SAR values (9.23 W/kg) were close to the International Electrotechnical Commission standard for normal level controlled scans.[40] Therefore, future work should focus on improving the isolation between the 2 RF coils in the magnet, for example, using passive *trap* circuits tuned to the ^{1}H resonance frequency on the ^{129}Xe RF coil.[41] The obtained results show some improvement when compared with

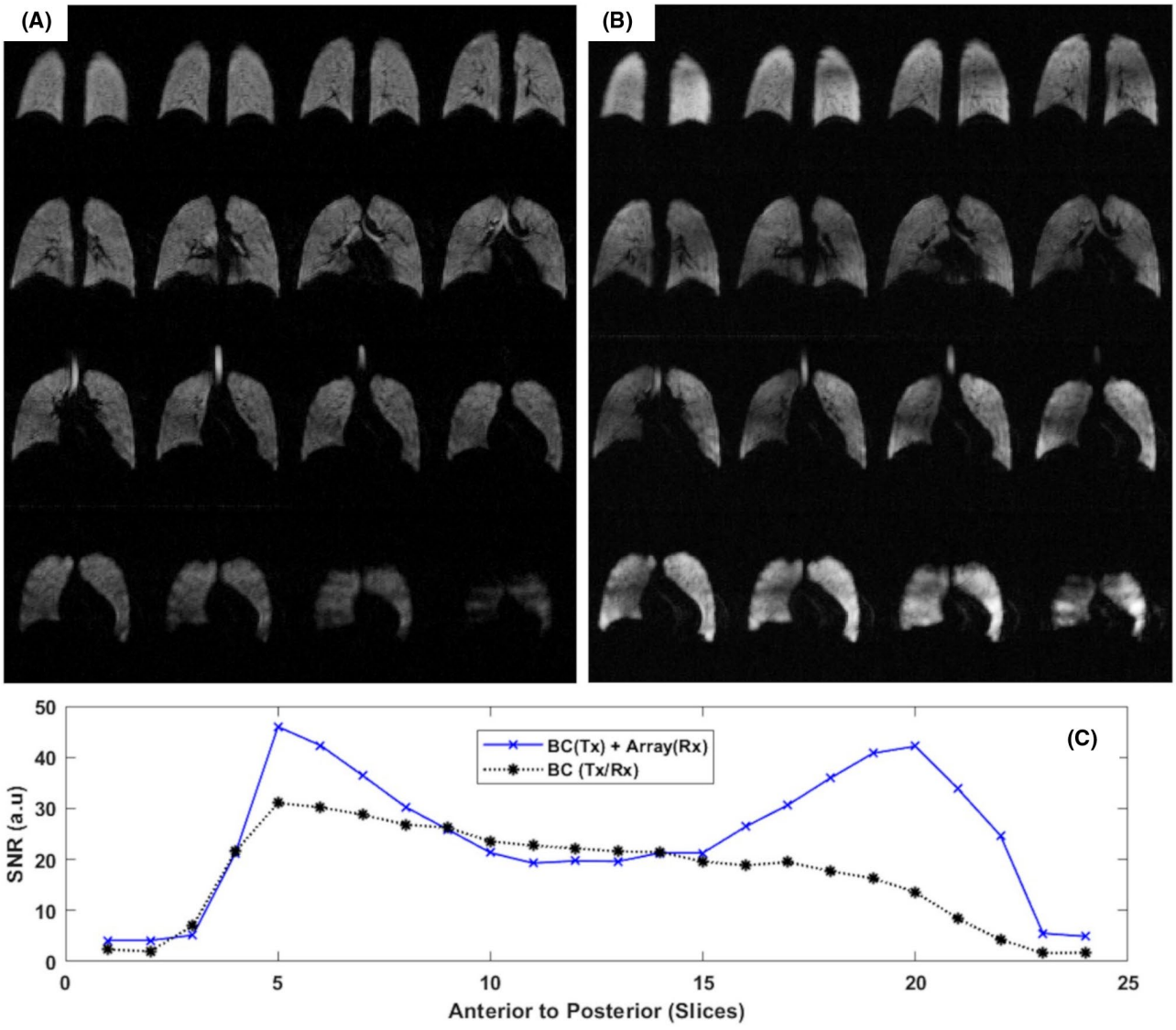

FIGURE 4 Ventilation images obtained with (A) the asymmetrical birdcage in transceiver configuration and (B) 8-channel receiver RF coils array. (C) Comparison of averaged SNR of each coronal slice for the 2 RF configurations

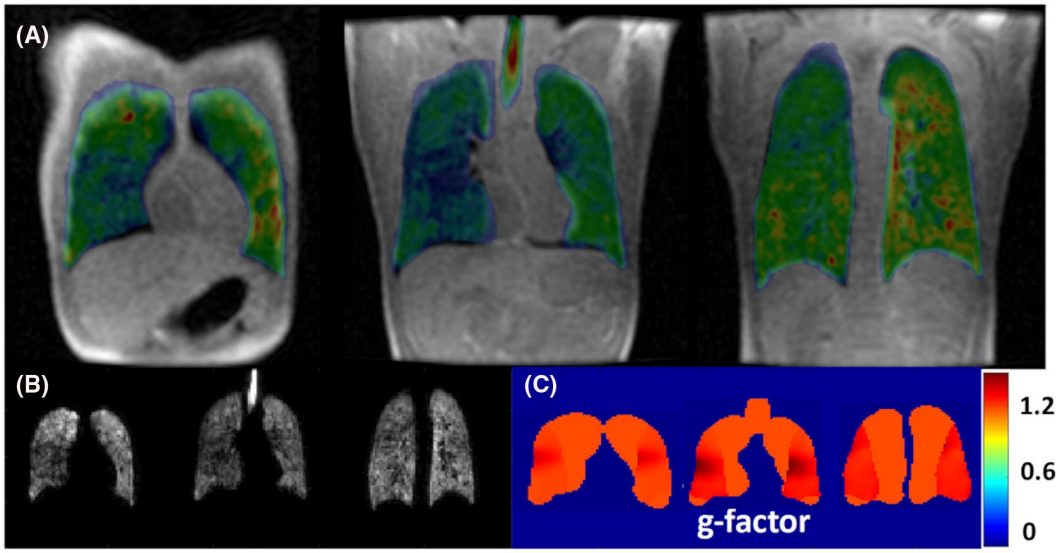

FIGURE 5 (A) ^{1}H Anatomical and coregistered with HP ^{129}Xe ventilation images. (B) Accelerated images and (C) g factor maps for acceleration factor of 2

the B_1 field homogeneity obtained with flexible vest coil designs similar to results previously reported in literature.[24,25] When combined with a separate 8-channel receive array, the increased SNR was evident despite some dropoff in the sensitivity toward the central slices. The receiver RF coil array permitted acceleration of 2 with low g-factor values (maximum values ~1.4).

5 | CONCLUSION

We have demonstrated an RF coil setup for ^{129}Xe human lung imaging at 1.5 T using an asymmetrical elliptical ^{129}Xe birdcage RF coil both as a transceiver and with a receive-only RF coil array. This ^{129}Xe birdcage RF coil, designed without an RF shield and with receive-only RF coil array compatibility, has enabled both ^{1}H MR imaging and accelerated imaging, functionality which has not been previously demonstrated together.

ACKNOWLEDGMENT

Funding was provided by The Medical Research Council (MRC) grant MR/M008894/1.

CONFLICT OF INTEREST

Coauthor (F.R.) is an employee of GE Healthcare. No funds, instructions or directions from the industry (GE Healthcare or any other company) were provided for this specific project. Several proprietary components, assemblies and consumables were purchased from GE Healthcare through a long-standing broader collaboration.

ORCID

Claudio Puddu https://orcid.org/0000-0003-1444-3112
Madhwesha Rao https://orcid.org/0000-0002-4109-4176
Guilhem Collier https://orcid.org/0000-0002-1874-4775
Adam Maunder https://orcid.org/0000-0002-1161-8741
Ho-Fung Chan https://orcid.org/0000-0002-5382-2097
Nicola De Zanche https://orcid.org/0000-0003-4424-8430

REFERENCES

1. Ebert M, Grossmann T, Heil W, et al. Nuclear magnetic resonance imaging with hyperpolarised helium-3. *Lancet*. 1996;347:1297-1299.
2. Albert MS, Cates GD, Driehuys B, et al. Biological magnetic resonance imaging using laser-polarized 129Xe. *Nature*. 1994;370:199-201.
3. Walkup LL, Thomen RP, Akinyi TG, et al. Feasibility, tolerability and safety of pediatric hyperpolarized 129Xe magnetic resonance imaging in healthy volunteers and children with cystic fibrosis. *Pediatr Radiol*. 2016;46:1651-1662.
4. Lutey BA, Lefrak SS, Woods JC, et al. Hyperpolarized 3 He MR imaging: physiologic monitoring observations and safety considerations in 100 consecutive subjects. *Radiology*. 2008;248:655-661.
5. Kirby M, Parraga G. Pulmonary functional imaging using hyperpolarized noble gas MRI. Six years of start-up experience at a single site. *Acad Radiol*. 2013;20:1344-1356.
6. Woodhouse N, Wild JM, van Beek EJR, Hoggard N, Barker N, Taylor CJ. Assessment of hyperpolarized 3 He lung MRI for regional evaluation of interventional therapy: a pilot study in pediatric cystic fibrosis. *J Magn Reson Imaging*. 2009;30:981-988.
7. Swift AJ, Wild JM, Fichele S, et al. Emphysematous changes and normal variation in smokers and COPD patients using diffusion 3He MRI. *Eur J Radiol*. 2005;54:352-358.

8. van Beek EJR, Wild JM, Kauczor H-U, Schreiber W, Mugler JP, de Lange EE. Functional MRI of the lung using hyperpolarized 3-helium gas. *J Magn Reson Imaging*. 2004;20:540-554.
9. Xu X, Norquay G, Parnell SR, et al. Hyperpolarized 129 Xe gas lung MRI-SNR and T2* comparisons at 1.5 T and 3 T. *Magn Reson Med*. 2012;68:1900-1904.
10. Narazaki M, Kimura A, Wakayama T, Imai H, Fujiwara H. Origin of dissolved-phase hyperpolarized 129Xe signal in the mouse chest based on experimental evidence from extensive magnetic resonance measurements. *Magn Reson Med Sci*. 2011;10:149-154.
11. Kaushik SS, Freeman MS, Cleveland ZI, et al. Probing the regional distribution of pulmonary gas exchange through single-breath gas- and dissolved-phase 129Xe MR imaging. *J Appl Physiol*. 2013;115:850-860.
12. Cleveland ZI, Cofer GP, Metz G, et al. Hyperpolarized 129Xe MR imaging of alveolar gas uptake in humans. *PLoS One*. 2010;5:e12192.
13. Wang JM, Robertson SH, Wang Z, et al. Using hyperpolarized 129Xe MRI to quantify regional gas transfer in idiopathic pulmonary fibrosis. *Thorax*. 2018;73:21-28.
14. Chacon Caldera J, Maunder A, Rao M, et al. Dynamic MRI of hyperpolarized Xenon-129 uptake in the human kidney using a dedicated transmission-only-reception-only array at 3 Tesla. In Proceedings of the 26th Annual Meeting of ISMRM, Paris, France, 2018. Abstract 4470.
15. Chacon-Caldera J, Maunder A, Rao M, et al. Dissolved hyperpolarized xenon-129 MRI in human kidneys. *Magn Reson Med*. 2020;83:262-270.
16. Miller G, Cates G, Keder D, et al. Dynamic spectroscopy of dissolved-phase xenon-129 in the human kidney. In Proceedings of the 25th Annual Meeting of ISMRM, Honolulu, HI, 2017. Abstract 1182.
17. Rao M, Stewart NJ, Norquay G, Griffiths PD, Wild JM. High resolution spectroscopy and chemical shift imaging of hyperpolarized 129 Xe dissolved in the human brain in vivo at 1.5 Tesla. *Magn Reson Med*. 2016;75:2227-2234.
18. Rao M, Stewart NJ, Griffiths PD, Norquay G, Wild JM. Imaging human brain perfusion with inhaled hyperpolarized 129Xe MR imaging. *Radiology*. 2018;286:659-665. doi: 10.1148/radiol.2017162881.
19. Hane F, Li T, Plata J-A, Hassan A, Granberg K, Albert M. Inhaled xenon washout as a biomarker of Alzheimer's disease. *Diagnostics (Basel)*. 2018;8:41.
20. De Zanche N, Chhina N, Teh K, Randell C, Pruessmann KP, Wild JM. Asymmetric quadrature split birdcage coil for hyperpolarized 3He lung MRI at 1.5T. *Magn Reson Med*. 2008;60:431-438.
21. Wetterling F, Corteville DM, Kalayciyan R, et al. Whole body sodium MRI at 3T using an asymmetric birdcage resonator and short echo time sequence: first images of a male volunteer. *Phys Med Biol*. 2012;57:4555-4567.
22. Farag A, Peterson JC, Szekeres T, et al. Unshielded asymmetric transmit-only and endorectal receive-only radiofrequency coil for ^{23}Na MRI of the prostate at 3 Tesla. *J Magn Reson Imaging*. 2015;42:436-445.
23. Deppe MH, Parra-Robles J, Marshall H, Lanz T, Wild JM. A flexible 32-channel receive array combined with a homogeneous transmit coil for human lung imaging with hyperpolarized 3He at 1.5 T. *Magn Reson Med*. 2011;66:1788-1797.
24. Dregely I, Ruset IC, Wiggins G, et al. 32-channel phased-array receive with asymmetric birdcage transmit coil for hyperpolarized xenon-129 lung imaging. *Magn Reson Med*. 2013;70:576-583.
25. De Zanche N, Chhina N, Teh K, Randell C, Wild JM. Optimized asymmetric quadrature split birdcage coil for hyperpolarized 3 He lung MRI at 1.5T. In Proceedings of the 15th Annual Meeting of ISMRM, Berlin, Germany, 2007. p. 240.
26. Collins CM, Smith MB. Calculations of B1 distribution, SNR, and SAR for a surface coil adjacent to an anatomically-accurate human body model. *Magn Reson Med*. 2001;45:692-699.
27. Horn FC, Rao M, Stewart NJ, Wild JM. Multiple breath washout of hyperpolarized 129 Xe and 3 He in human lungs with three-dimensional balanced steady-state free-precession imaging. *Magn Reson Med*. 2017;77:2288-2295.
28. Walker TG, Happer W. Spin-exchange optical pumping of noble-gas nuclei. *Rev Mod Phys*. 1997;69:629-642.
29. Norquay G, Collier GJ, Rao M, Stewart NJ, Wild JM. 129Xe-Rb spin-exchange optical pumping with high photon efficiency. *Phys Rev Lett*. 2018;15:121.
30. Deoni SCL. High-resolution T1 mapping of the brain at 3T with driven equilibrium single pulse observation of T1 with high-speed incorporation of RF field inhomogeneities (DESPOT1-HIFI). *J Magn Reson Imaging*. 2007;26:1106-1111.
31. Gudbjartsson H, Patz S. The Rician distribution of noisy MRI data. *Magn Reson Med*. 1995;34:910-914.
32. Roemer PB, Edelstein WA, Hayes CE, Souza SP, Mueller OM. The NMR phased array. *Magn Reson Med*. 1990;16:192-225.
33. McKenzie CA, Yeh EN, Ohliger MA, Price MD, Sodickson DK. Self-calibrating parallel imaging with automatic coil sensitivity extraction. *Magn Reson Med*. 2002;47:529-538.
34. Weiger M, Pruessmann KP, Boesiger P. 2D SENSE for faster 3D MRI. *MAGMA*. 2002;14:10-19.
35. Wang J, Mao W, Qiu M, Smith MB, Constable RT. Factors influencing flip angle mapping in MRI: RF pulse shape, slice-select gradients, off-resonance excitation, and B0 inhomogeneities. *Magn Reson Med*. 2006;56:463-468.
36. Wild JM, Teh K, Woodhouse N, et al. Steady-state free precession with hyperpolarized 3He: experiments and theory. *J Magn Reson*. 2006;183:13-24.
37. Bieri O, Scheffler K. Fundamentals of balanced steady state free precession MRI. *J Magn Reson Imaging*. 2013;38:2-11.
38. Mugler JP, Altes TA. Hyperpolarized 129 Xe MRI of the human lung. *J Magn Reson Imaging*. 2013;37:313-331.
39. Farag A, Wang J, Ouriadov A, Parraga G, Santyr G. Unshielded and asymmetric RF transmit coil for hyperpolarized 129Xe human lung imaging at 3.0 T. In Proceedings of the 20th Annual Meeting of ISMRM, Melbourne, Australia, 2012. p. 1361.
40. International Electrotechnical Commission (IEC). *IEC 60601-2-33:2010 Medical Electrical Equipment - Part 2-33: Particular Requirements for the Basic Safety and Essential Performance of Magnetic Resonance Equipment for Medical Diagnosis*. https://webstore.iec.ch/publication/2647. Accessed October 31, 2020.
41. Rao M, Robb F, Wild JM. Dedicated receiver array coil for 1H lung imaging with same-breath acquisition of hyperpolarized 3He and 129Xe gas. *Magn Reson Med*. 2015;74:291-299.

How to cite this article: Puddu C, Rao M, Xu X, et al. An asymmetrical whole-body birdcage RF coil without RF shield for hyperpolarized ^{129}Xe lung MR imaging at 1.5 T. *Magn Reson Med*. 2021;00:1–9. https://doi.org/10.1002/mrm.28915